International Symposium
On Turbulence and Shear Flow
Phenomena (TSFP-9)
June 30 - July 3, 2015 *Melbourne, Australia*

ADAPTIVE CONTROL OF FINITE-AMPLITUDE 3D DISTURBANCES IN 2D BOUNDARY-LAYER FLOWS

Nicolò Fabbiane
Department of Mechanics
Linnè FLOW Centre
Royal Institute of Technology (KTH)
Stockholm S-10044, Sweden
nicolo@mech.kth.se

Shervin Bagheri
Department of Mechanics
Linnè FLOW Centre
Royal Institute of Technology (KTH)
Stockholm S-10044, Sweden
shervin@mech.kth.se

Dan S. Henningson
Department of Mechanics
Linnè FLOW Centre
Royal Institute of Technology (KTH)
Stockholm S-10044, Sweden
henning@mech.kth.se

ABSTRACT

Friction drag is reduced in a two-dimensional (2D) boundary-layer flow by delaying the laminar-to-turbulence transition. A localised forcing in the wall region is used to attenuate the growing 3D disturbances that eventually trigger the turbulent regime farther downstream. An adaptive filtered-X least-mean-squared (FXLMS) algorithm is used to process the information of the flow gathered from two rows of surface hot-wires sensors and compute the forcing, performed by a row of plasma actuators. LES simulations are used to evaluate and analyze the performance of the described control strategy: in particular, a study on the streamwise position of the sensor and an actual transition delay scenario are presented.

1 INTRODUCTION

Being able to reduce the friction drag in boundary-layer flows may reduce the energy and fuel consumption required for transportation, such as trains and airplanes. Since the laminar state is characterized by a smaller friction drag than the turbulent one, avoiding or delaying the laminar-to-turbulence transition will reduce the overall drag. In a low-turbulence environment, the transition is dominated by local instabilities of the flow – Tollmien-Schlichting waves – that exponentially grow, eventually breakdown and lead to turbulence (Saric *et al.*, 2002).

Reactive control technique have been studied in order to delay the laminar-to-turbulence transition (Sturzebecher & Nitsche, 2003; Lundell, 2007; Bagheri & Henningson, 2011). In particular, the work by Semeraro *et al.* (2013) showed that is possible to control a finite-amplitude single wave-packet by using model-based control techniques. Although a clear transition to turbulence was observed in the uncontrolled case, a real disturbance environment is more complex and many 3D disturbances interact with each other. In this work, instead, a a complex 3D random pattern of disturbances is generated by using a span-wise row of independent random forcings d (Figure 1). Each input is has a localised spatial support inside the boundary-layer.

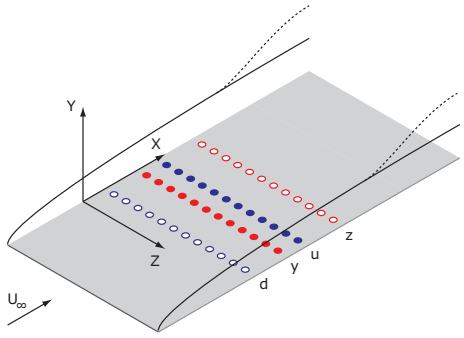

Figure 1. Control set-up. Random 3D disturbances are generated by a row of localised independent forcings d. The measurements from the sensors y and z are used by an adaptive FXLMS algorithm to compute the actuation signal for the actuators u in order to reduce the amplitude of the detected disturbances.

The recent numerical and experimental studies by Fabbiane *et al.* (2015) highlighted that a model-based approach can be sensitive to model inaccuracies when compared to adaptive-control techniques. Hence, an adaptive multiple-input-multiple-output (MIMO) FXLMS compensator is considered in this work: this algorithm is an extension of the single-input-single-output (SISO) algorithm used by Sturzebecher & Nitsche (2003) in their experimental investigation on 2D disturbance control.

2 CONTROL STRATEGY

The control action is performed by a row of localized, equispaced actuators forcing the flow in the proximity of

the wall. Their action $u_l(t)$ is computed based on the measurements $y_m(t)$ by a row of sensors upstream the actuators: for this set-up, the number of sensors is equal to the number of actuators and they are positioned aligned respect the flow direction (Figure 2).

We assume a linear control law and an equal number (M) of sensors and actuators. As a consequnce, the number of transfer function between the M sensors y_m and the actuators u_l is M^2. This imposes a computation constraint when M is large, which is the case when covering a large spanwise width with the controller. However, since the flow is spanwise homogeneous, the same transfer K_m function from all the sensors y_l to one actuator is replicated for each actuator u_m, as shown in Figure 2. This assumption reduces the number of transfer function to be designed from M^2 to M. Hence, the finite impulse response (FIR) filter representation of the control law reads

$$u_l(n) = \sum_m \sum_j K_m(j)\, y_{m+l}(n-j) \quad \forall l \tag{1}$$

where $u_l(n)$ and $y_l(n)$ are the time-discrete control and measurement signals, $K_m(j) \in \mathbb{R}^{M\times N}$ is the convolution kernel of the compensator and $N\Delta t$ is the time-horizon of the FIR filter (Aström & Wittenmark, 1995; Fabbiane *et al.*, 2014).

The design of the compensator consists in computing the time-discrete convolution kernel $K_m(j)$. In this work, A MIMO version of the FXLMS algorithm introduced by Sturzebecher & Nitsche (2003) is used to dynamically design the compensator. The algorithm aims to minimise the sum of the squared measurement signals $z_l(n)$:

$$\min_{K_m} \left(\sum_l z_l^2(n) \right). \tag{2}$$

Hence the kernel is updated via a steepest descend algorithm at each time step:

$$K_m(i|n+1) = K_m(i|n) - \mu\, \lambda_m(i|n). \tag{3}$$

where the descend direction $\lambda_m(j|n)$ is given by

$$\lambda_m(i|n) = \frac{\partial \left(\sum_l z_l^2(n)\right)}{\partial K_m(i)} = 2 \sum_l z_l(n)\, \frac{\partial z_l(n)}{\partial K_m(i)}. \tag{4}$$

In order to compute the derivative in the previous equation, it is necessary to explicit $z(n)$ dependencies:

$$\begin{aligned} z_l(n) &= \sum_r \sum_j P_{zd,r}(j)\, d_{r+l}(n-j) + \sum_r \sum_j P_{zu,r}(j)\, u_{r+l}(n-j) = \\ &= [\cdots] + \sum_r \sum_j P_{zu,r}(j) \sum_m \sum_i K_m(i)\, y_{m+r+l}(n-j-i) = \\ &= [\cdots] + \sum_m \sum_i K_m(i) \sum_r \sum_j P_{zu,r}(j)\, y_{r+m+l}(n-j-i) = \\ &= [\cdots] + \sum_m \sum_i K_m(i)\, f_{m+l}(n-i), \end{aligned} \tag{5}$$

where the same span-wise homogeneity assumption has been made for the plant kernels $P_{zd,r}(j)$ and $P_{zu,r}(j)$ that represent the transfer functions $d_r \to z_l$ and $u_r \to z_l$ respectively. Hence the descend direction reads

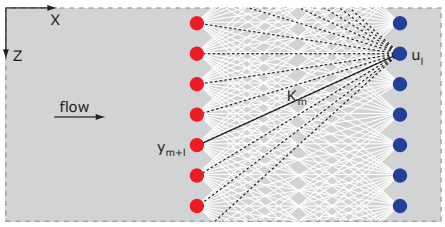

Figure 2. Compensator structure. The action of each actuator u_m is computed by filtering the signals from all the sensor y_l via a linear filter K_m. An adaptive FXLMS filter is responsible of computing the K_m response in order to maximize in real time the control performances measured by the error sensors z_l.

$$\lambda_m(i|n) = 2 \sum_l z_l(n)\, \frac{\partial z_l(n)}{\partial K_m(i)} = 2 \sum_l z_l(n) f_{m+l}(n-i). \tag{6}$$

Note that this method is not completely model free as $P_{l+m}(i)$ is needed to compute $f_l(n)$.

3 DNS/LES SIMULATIONS

In order to analyze the control algorithm, LES simulations are performed using a pseudo-spectral code (Chevalier *et al.*, 2007). Periodicity is assumed in the spanwise and streamwise directions: a fringe-region is placed in the last 20% of the domain to enforce the periodicity in the streamwise direction. The flow is expanded over 1536×384 Fourier modes in the XZ plane and 101 Chebyshev's polynomials in the wall-normal direction. The computational domain Ω extends for $[0,2000) \times [0,30] \times [-125,125)$ in the X, Y and Z direction. All the spatial dimensions are non-dimensionalized by the boundary-layer displacement thickness in the beginning of the domain δ_0. The resulting Reynolds number is defined as $Re = U\delta_0/\nu = 1000$, where U is the free-stream velocity and ν the kinematic viscosity. For the time-integration a Crank-Nicholson/Runge-Kutta method is used with a constant time-step $\Delta t = 0.4\delta_0/U$.

Disturbance sources in the beginning of the domain are modelled according to Semeraro *et al.* (2013), while plasma actuators are considered to perform the control action and modelled via a volume forcing (Kriegseis *et al.*, 2013). In this set-up, 25 equispaced objects for each row of sensors/actuators/disturbances are considered with a spanwise separation $\Delta Z = 10$, accordingly to the work by (Semeraro *et al.*, 2013).

4 SENSORS POSITION

The relative streamwise position between sensors and actuators has been studied via linear DNS simulations on a reduction of the original domain, $(X,Y,Z) \in [0,1000) \times [0,30] \times [-75,75)$. The spanwise separation between sensors/actuators $\Delta Z = 10$ is maintained, resulting in 15 objects for each sensors/actuators row. The actuators row is kept at $X_u = 400$: reference and errors sensors are moved instead

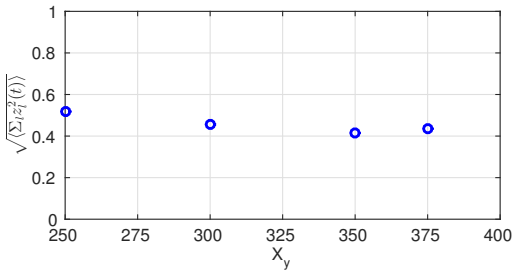

Figure 3. Reference sensor position. $\sqrt{\langle \Sigma_l z_l^2 \rangle}$ is reported as a function of the reference-sensor streamwise position X_y. The reported values are normalised with respect to the uncontrolled case.

in order to maximize the performance of the control action. The root-mean-square of the error sensor is used as performance indicator: the closer to zero the more effective the disturbance attenuation.

Figure 5 report the performance of the control when the reference sensor (y_m) are moved, while the error sensors (z_l) are fixed at $X_z = 700$. The control action appears not to be particularly sensitive to the position of the reference sensor X_y. However, it is interesting the effect that X_y has on the control kernel: in Figure 4 the control kernel are shown for the tested y_l positions.

Each line indicates the transfer function $K_m(j)$ between the a generic actuator u_l and the sensor y_{m+l} that is positioned at $m\Delta Z$ respect to the actuator itself (Figure 2). The thicker line in each sub-figure shows the transfer function $K_0(j)$, i.e. the connection $y_m \rightarrow u_m$ between the sensor and the actuator positioned at the same Z location.

All kernels present a compact support along the spanwise direction: as the index m increases the magnitude of the transfer functions decays and it becomes zero for $m = \pm 5$. This means that the action of one actuator depends only on a limited number of sensors, between $Z = -50$ and $Z = 50$ with respect to the actuator position. This permits to reduce the number of transfer functions that have to be calculated and, as a consequence, the compensator computational cost.

Interestingly, all kernels share the same spanwise support and structure. The effect of the relative position $X_u - X_y$ seems to be reduced to a backward shift in time of the compensator response.This behaviour of the compensator response is due to the convective nature of this type of instabilities (Schmid & Henningson, 2001): time-delays, in fact, are a peculiar feature of the control of this type of flows. If we consider $K_0(j)$ – i.e. the connection between the sensor and the actuator positioned at the same Z location – in Figure 4(a), the maximum of the transfer function occurs at $j\Delta t \approx 250$, which corresponds to the time that a TS-wavepacket takes to travel from the sensor to the actuator location. As the reference sensor is moved downstream (Figure 4(b)-(d)), this time-delay is reduced and an increasing part of the original structure is not present any more.

In Figure 5 the positioning of the error sensors X_z is addressed. The control performances measured by the error sensors z_l improves as the sensors row is moved upstream, i.e. towards the actuator (blue circles). This result, however, can be misleading: the red squares report the performance of the control action measured by a fixed row of sensors r_l at $X_r = 750$. From this, it is clear that the compensator is performing worse as the error sensors row is moved closer

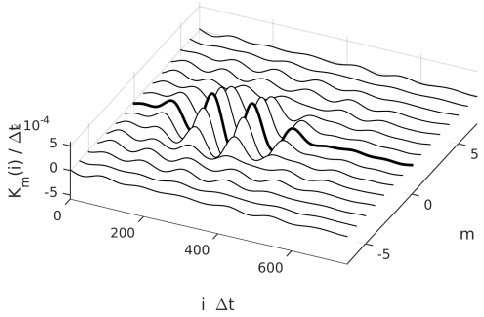

(a) $X_y = 300 \quad X_z = 700$

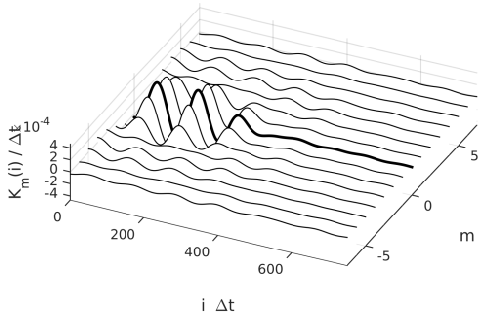

(b) $X_y = 350 \quad X_z = 700$

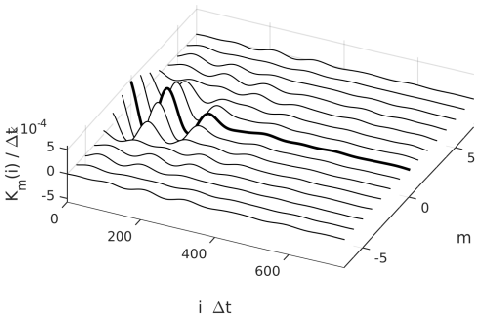

(c) $X_y = 375 \quad X_z = 700$

Figure 4. Convolution kernels $K_m(i)$ computed by FXLMS algorithm for different streamwise positions of the reference sensors X_y. The thick line indicates $K_0(i)$, i.e. the connection between the actuator and the sensor at the same Z location.

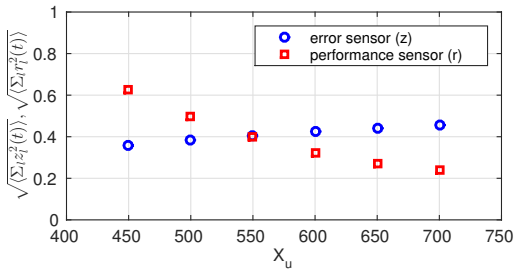

Figure 5. Error sensor position. The blue circles report $\sqrt{\langle \Sigma_l z_l^2 \rangle}$ as a function of the reference-sensor streamwise position X_y. The red dots report the same quantity for an additional fixed row of sensors (*performance sensors*) positioned at $X = 750$. The reported values are normalised with respect to the uncontrolled case.

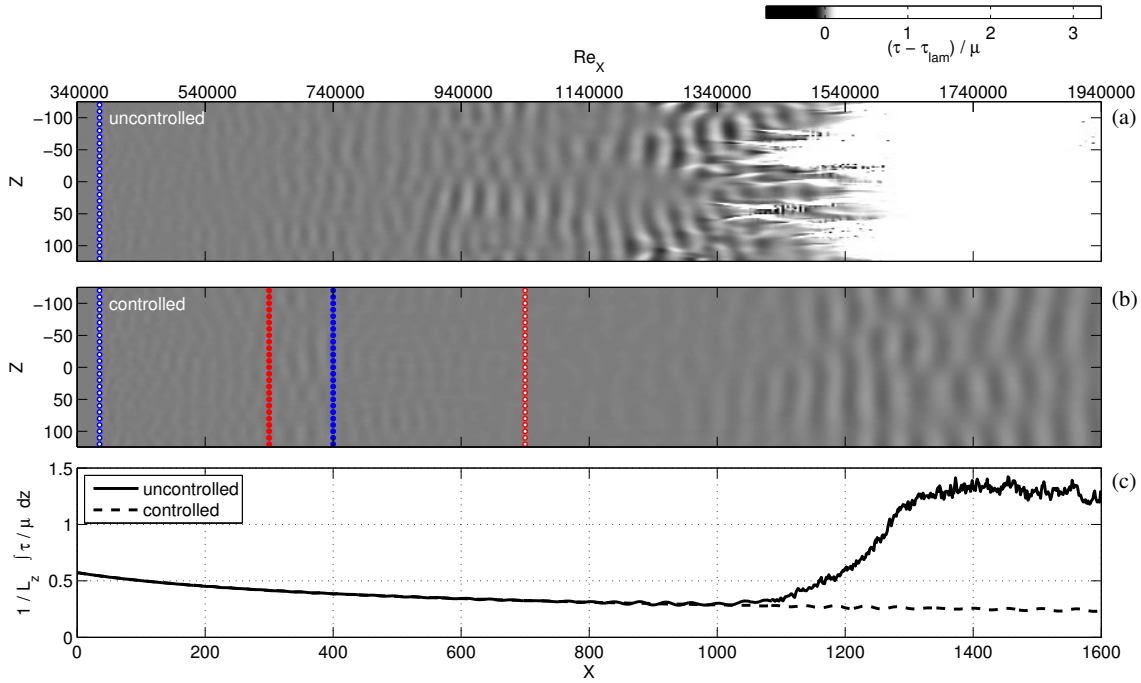

Figure 6. Transition delay. In (a) and (b) the skin friction fluctuations respect to the laminar solution are shown at $t = 4000\frac{\delta_0}{U}$. In the uncontrolled case (a) the disturbances grow and lead to transition to turbulent state in the end of the domain. In the controlled case (b), instead, the disturbances are attenuated by actuators action and transition is delayed, see also (c). The top axis reports $Re_X = \frac{U(X-X_{LE})}{\nu}$, where X_{LE} is the leading-edge position.

to the actuator. Hence, in the linear-perturbation limit, the better performances are given by the farthest position of the error sensor. However, if finite amplitude disturbances are considered, one may want to place as near as possible to the actuator in order lo limit the non-linear effects: a balance between the two concurring necessities.

5 TRANSITION DELAY

According to the results of the previous section, the reference sensor y_m are positioned at $X_y = 300$ and the error sensors z_l at $X_z = 700$, Figure 6(b). The perturbation is produced by 25 localised disturbances fed by 25 independent white noise signals $d_m(t)$ with variance $1/3 \cdot 10^{-3}$ each.

The transition delay performed by the compensator is shown in Figure 6. The friction-trace of the TS-waves generated by the disturbance source in the beginning of the domain is visible in Figure 6(a-b), where the skin instantaneous friction fluctuations respect to the laminar solution are reported. The disturbances exponentially grow while travelling downstream and lead to transition in the uncontrolled case. In Figure 6(b) it can bee seen that the compensator is able to attenuate those disturbances and move the transition point out of the computational box. In particular, friction fluctuations decay downstream the actuators, they reach a minimum amplitude where error sensor z_l are positioned and they grow again without triggering the transition. This can be seen also in Figure 6(c) where the spanwise average of the streamwise stress is shown: the area between the controlled and uncontrolled friction curves gives directly the drag-save per units of spanwise length that is obtained by applying the control.

6 CONCLUSIONS

The employed adaptive control technique is able to delay the transition point in a realistic scenario, as shown by the results reported in this short overview.

Some interesting features of the controller have been highlighted, e.g. the compact support of the kernel in the spanwise direction. As shown in Figure 4, each actuator action is dependent on a limited number of reference sensor along the spanwise direction. This results permits to limit the number of transfer functions that are needed to effectively perform the control action and, hence, reduce the computational cost of the algorithm.

The results presented in this abstract are characterized by a linear regime in the region of the flow where the control action takes place. However, the adaptive nature of the FXLMS algorithm may permit the compensator to successfully operate for higher amplitude disturbances.

Moreover, in contrast to the model-based approach by Semeraro *et al.* (2013), the compensator design requires no models of disturbance environment; the only modelling required is the input/output relation between the actuators u_m and the error sensors z_l. The reduced modelling and the adaptivity of this type of compensator make this control strategy suitable for realistic applications, where one lacks exact knowledge flow conditions, as shown by Fabbiane *et al.* (2015).

ACKNOWLEDGEMENTS

The authors acknowledge support the Swedish Research Council (VR-2012-4246, VR-2010-3910) and the Linné Flow Centre. Computer time was provided by High Performance Computing Center North (HPC2N).

REFERENCES

Aström, K. J. & Wittenmark, B. 1995 *Adaptive Control*, 2nd edn. Addison Wesley.

Bagheri, S. & Henningson, D. S. 2011 Transition delay using control theory. *Philos. Trans. R. Soc.* **369**, 1365–1381.

Chevalier, M., Schlatter, P., Lundbladh, A. & Henningson, D. S. 2007 A pseudo-spectral solver for incompressible boundary layer flows. *Tech. Rep.* TRITA-MEK 2007:07. KTH Mechanics, Stockholm, Sweden.

Fabbiane, N., Semeraro, O., Bagheri, S. & Henningson, D. S. 2014 Adaptive and Model-Based Control Theory Applied to Convectively Unstable Flows. *Appl. Mech. Rev.* **66** (6), 060801.

Fabbiane, N., Simon, B., Fischer, F., Grundmann, S., Bagheri, S. & Henningson, D. S. 2015 On the Role of Adaptivity for Robust Laminar-Flow Control. *J. Fluid Mech.* **767**, R1.

Kriegseis, J., Schwarz, C., Tropea, C. & Grundmann, S 2013 Velocity-Information-Based Force-Term Estimation of Dielectric-Barrier Discharge Plasma Actuators. *J. Phys. D* **46** (5), 055202.

Lundell, F. 2007 Reactive control of transition induced by free-stream turbulence: an experimental demonstration. *J. Fluid Mech.* **585**, 41–71.

Saric, W. S., Reed, H. L. & Kerschen, E. J. 2002 Boundary-layer Receptivity to Freestream Disturbances. *Ann. Rev. Fluid Mech.* **34** (1), 291–319.

Schmid, P. J. & Henningson, D. S. 2001 *Stability and Transition in Shear Flows*. *Applied Mathematical Sciences* v. 142. Springer-Verlag.

Semeraro, O., Bagheri, S., Brandt, L. & Henningson, D. S. 2013 Transition delay in a boundary layer flow using active control. *J. Fluid Mech.* **731** (9), 288–311.

Sturzebecher, D. & Nitsche, W. 2003 Active cancellation of Tollmien–Schlichting instabilities on a wing using multi-channel sensor actuator systems . *Intl J. Heat and Fluid Flow* **24**, 572–583.